Electronic Supplementary Material (ESI) for Energy & Environmental Science.

Supplementary figures and text for

High-rate cycling in 3D dual-doped NASICON architectures toward room-temperature sodium-metal-anode solid-state batteries

*Prem Wicram Jaschin, Christopher R. Tang and Eric D. Wachsman**

Department of Materials Science and Engineering, University of Maryland, College Park, Maryland20742, United States

Maryland Energy Innovation Institute, University of Maryland, College Park, Maryland20742, United States

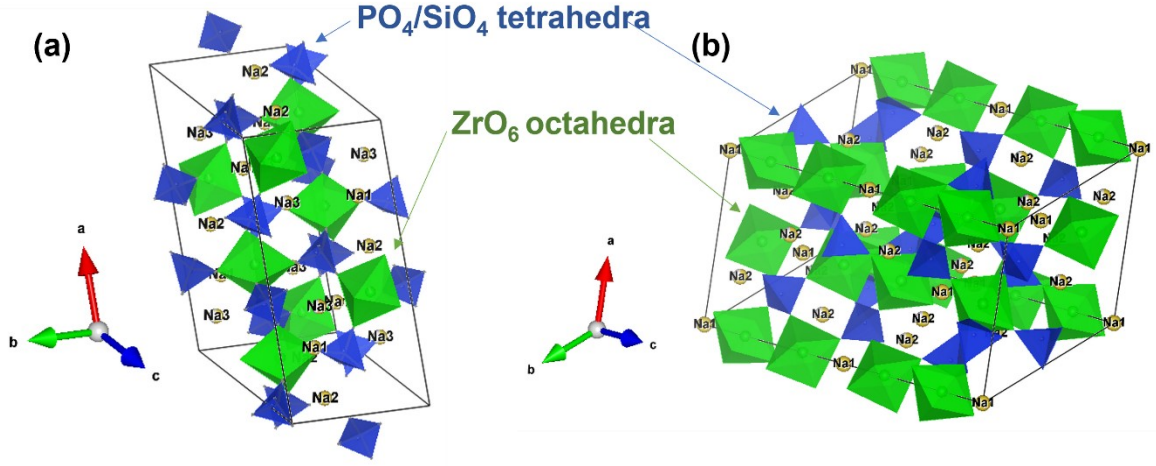

Figure S1 *(a) Monoclinic and (b) rhombohedral crystal structures of NASICON*

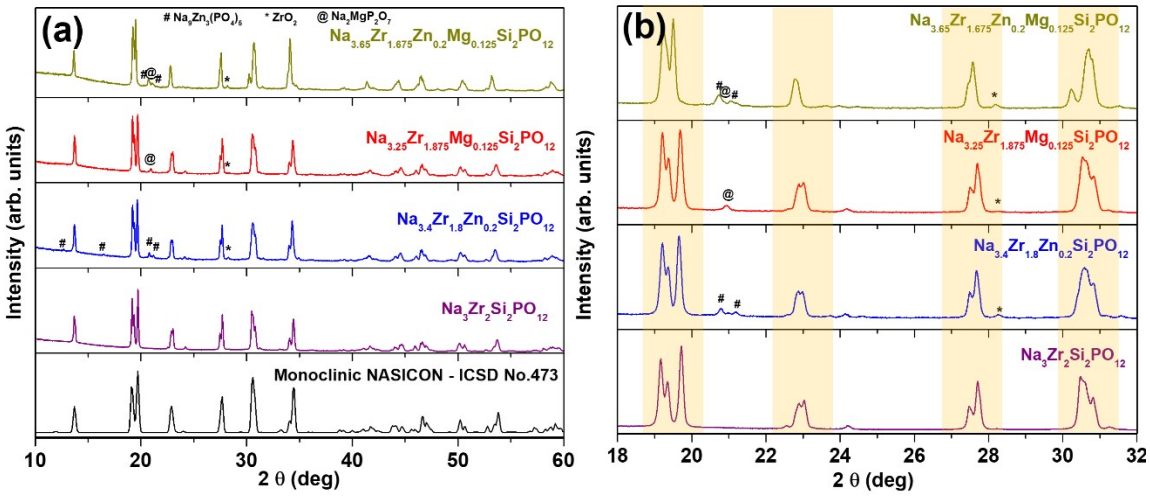

Figure S2. *(a) Powder X-ray diffraction patterns and (b) enlarged XRD patterns of undoped and doped NASICON powder after sintering.*

All the polycrystalline XRD profiles match the monoclinic phase of NASICON (ICSD No. 473) associated with the space group *C* 2/*c*. There were no impurity phases observed in the XRD patterns corresponding to the undoped NASICON sample. However, as the dopants were introduced into the NASICON structure, small fractions of impurity phases were observed. The Zn-dopant led to the segregation of $Na_3Zn_3(PO_4)_5$, whereas Mg-dopant resulted in the formation of $Na_2MgP_2O_7$ secondary phases. Dual-doped NASICON yielded a combined precipitation of both the aforementioned phases in the system. Traces of ZrO_2 were also observed in the doped NASICON samples. With the introduction of Zn- and Mg-dopants, the shifts in the diffraction peaks at 19.1° and 30.5° slightly shift to higher angles, while those at 19.5° and 34.2° shift to lower angles (as shown in Figure 2 (b)). Moreover, the shoulder peak at around 19° merges into a single and the peak at 30.5° splits into two peaks. These peak shifts in the XRD patterns of the doped-NASICON suggest that there is a clear structural transition from monoclinic phase to rhombohedral phase occurring in the system.

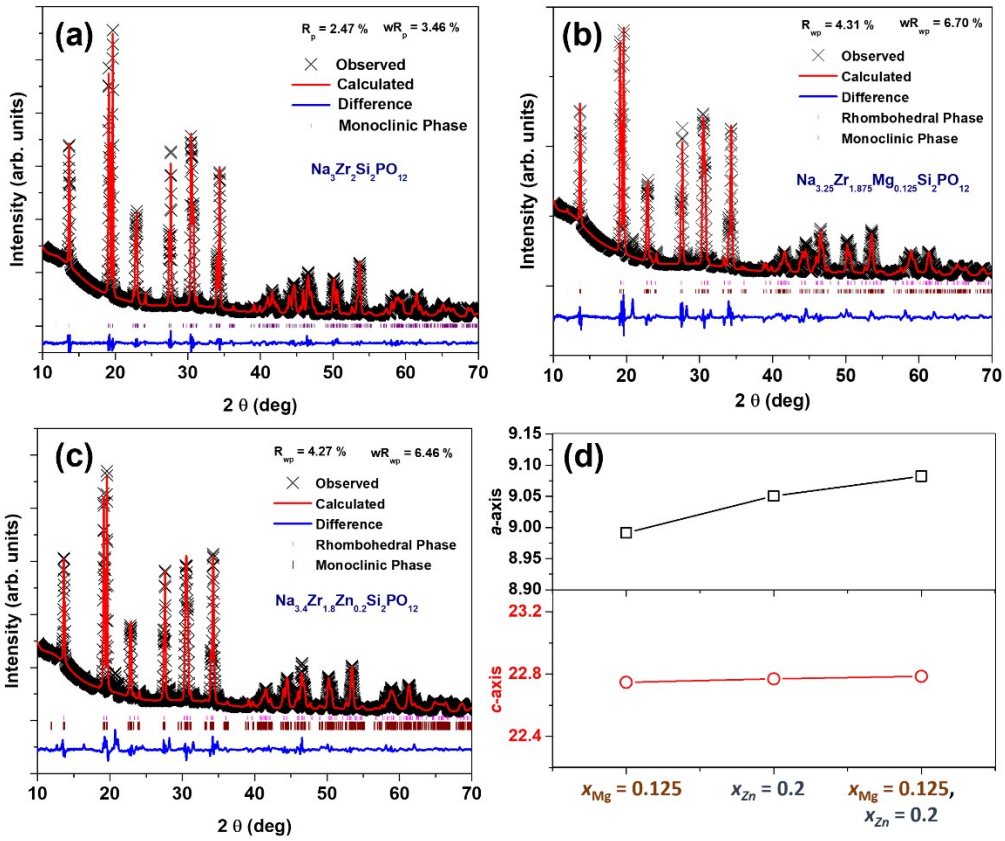

Figure S3 *Reitveld refined XRD patterns of (a) $Na_{3.25}Zr_{1.875}Mg_{0.125}Si_2PO_{12}$ and (b) $Na_{3.4}Zr_{1.8}Zn_{0.2}Si_2PO_{12}$. (c) Variation of rhombohedral parameters as a function of dopant ions determined from refinement.*

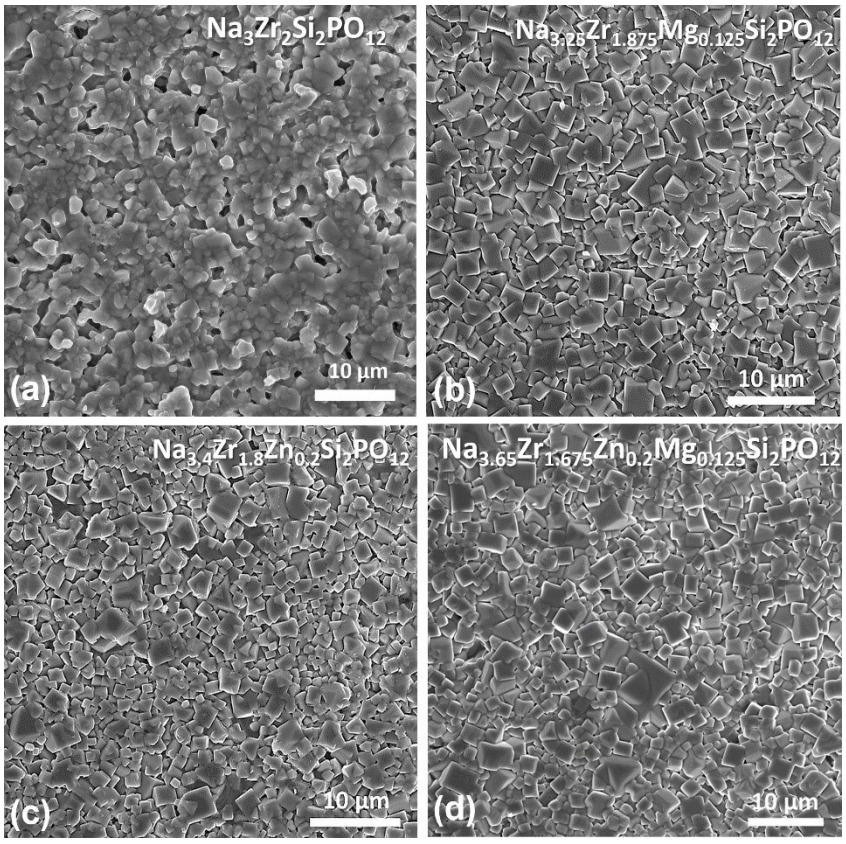

Figure S4 *SEM images of the surface microstructures of sintered pellets corresponding to compositions (a) $Na_{3.25}Zr_{1.875}Mg_{0.125}Si_2PO_{12}$ and (b) $Na_{3.4}Zr_{1.8}Zn_{0.2}Si_2PO_{12}$.*

The heat-treated pellet of the undoped NASICON sample is visibly less dense with the presence of a few pores and shows grains (of average size 1 µm) that appear held together by a continuous glassy phase across the crystallites. However, with the addition of the dopants into the NASICON system, the crystallites gain a uniform cubic shape and are well packed. Different grain sizes could be observed, with sizes varying from 1 µm sized smaller grains and all the way up to 10 µm. The average grain size for the dense pellets corresponding to the dual doped NASICON system was found to be around 4 µm (four times that of undoped samples). The introduction of the dual dopants appears to aid the sintering process by densification and grain growth.

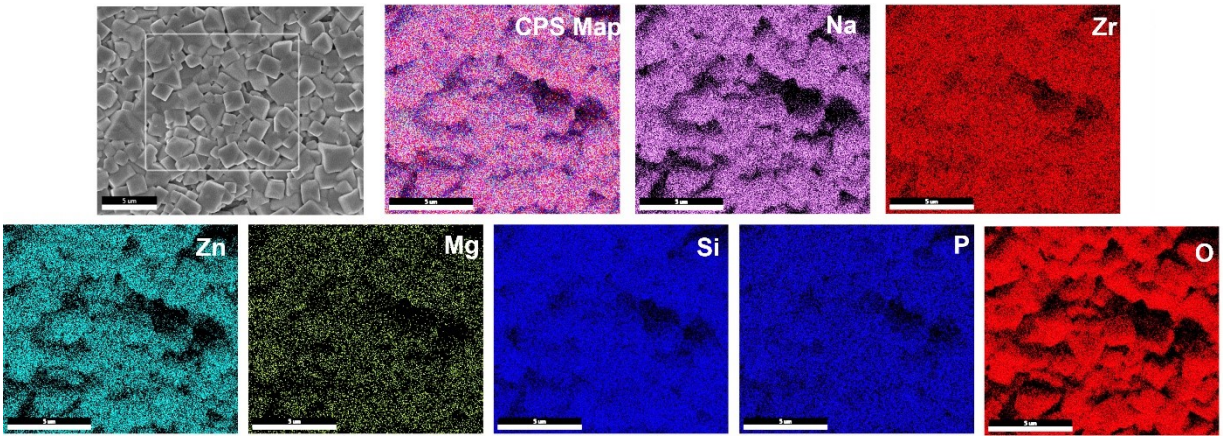

Figure S5 *EDS map depicting elemental distribution in Zn,Mg-codoped NASICON ceramic pellet.*

The results of EDS mapping on the dual-doped NASICON reveal that the distribution of elements including Na, Zr, Zn, Mg, Si, P, and O are quite uniform. There was no distinct segregation of phases observed through EDS mapping.

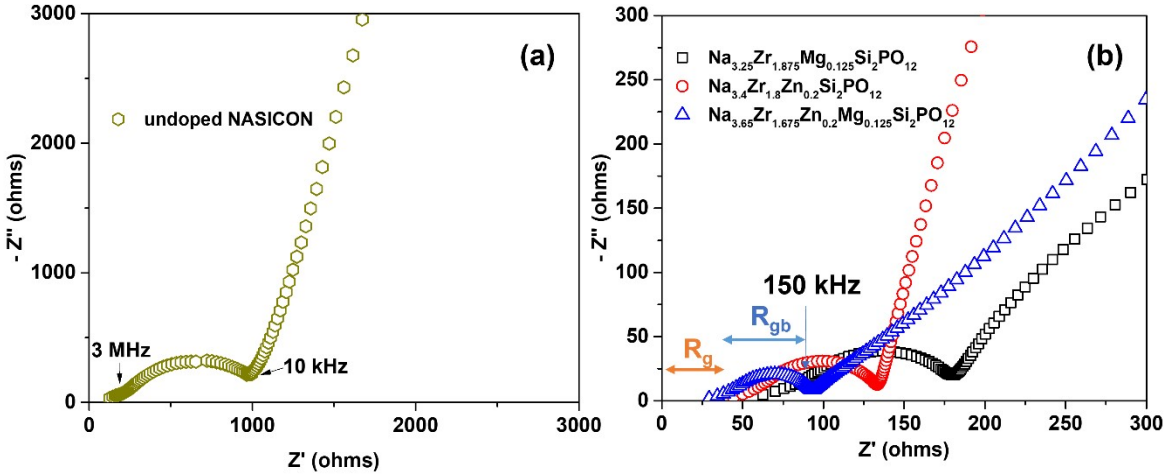

Figure S6 *Nyquist plots of (a) undoped- and (b) doped-NASICON ceramic pellets with blocking electrodes recorded at room temperature.*

Nyquist plots (imaginary vs real parts of the complex impedance) are imperative in identifying the individual contributions to the net ionic conductivity of the material. The room temperature Nyquist plots of the undoped- and doped-NASICON dense pellets are shown in Figure S6. Typical depressed semi-circles at high frequencies, followed by the capacitance tail (from the gold blocking electrodes) at lower frequencies were observed from all the samples. Only one semi-circle away from the origin was observed at high frequency (> 150 kHz), that is associated with grain-boundary contribution to total ionic conductivity. The semi-circle corresponding to the grain (bulk) conductivity is left unrealized due to the limitations of recording impedance above 7 MHz. Hence, the difference between the origin and the beginning of the first semi-circle is considered as the grain contribution. The semi-circle was fit using Zview with equivalent circuit consisting of a resistance (grain) in series with an RQ_{CPE} (grain boundary) element followed by CPE element to account for the low frequency tail.

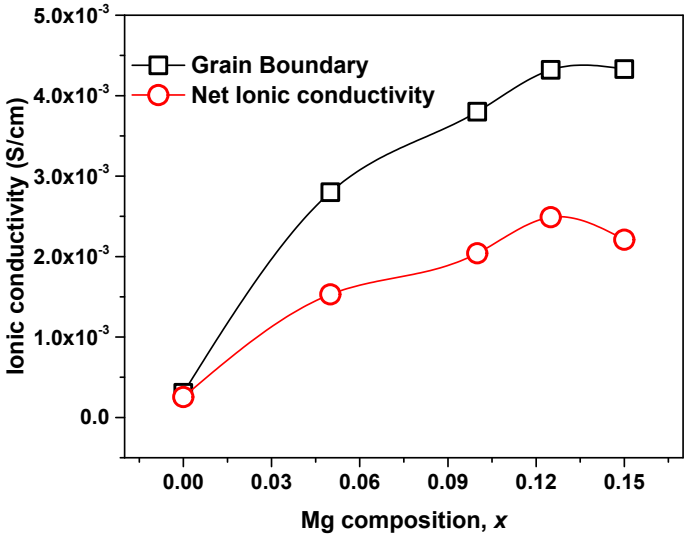

Figure S7 *Variation of grain boundary and total ionic conductivities as a function of Mg^{2+}-ion concentration in $Na_{3.4+2y}Zr_{1.8-y}Zn_{0.2}Mg_ySi_2PO_{12}$.*

With a constant Zn^{2+}-ion composition at x_{Zn} = 0.2, the Mg^{2+}-ion content was varied to determine the optimum co-dopant levels to achieve highest possible net ionic conductivity. Four compositions of Mg^{2+}-ion were studied – y_{Mg} = 0.05, 0.1, 0.125, 0.15 – in the process. The optimized composition of NASICON was determined to be $Na_{3.65}Zr_{1.675}Zn_{0.2}Mg_{0.125}Si_2PO_{12}$.

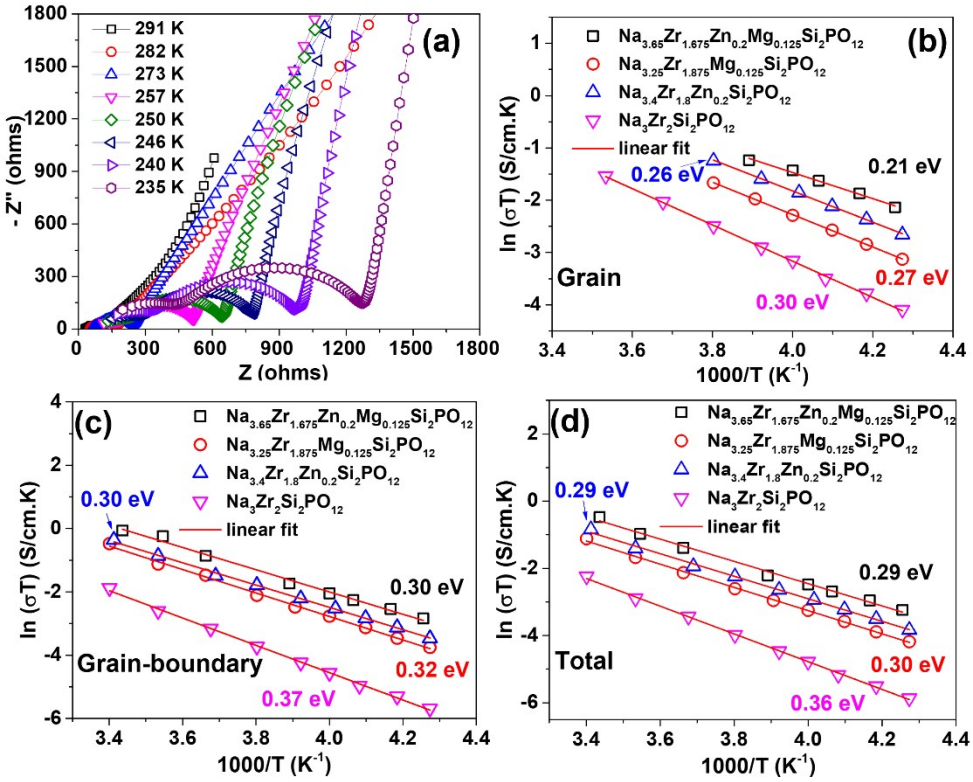

Figure S8 (a) *Nyquist plots of Zn,Mg-dual doped NASICON ceramic pellet as a function of temperature. Arrhenius plots of undoped and doped-NASICON based on (b) grain, (c) grain-boundary and (d) total ionic contributions.*

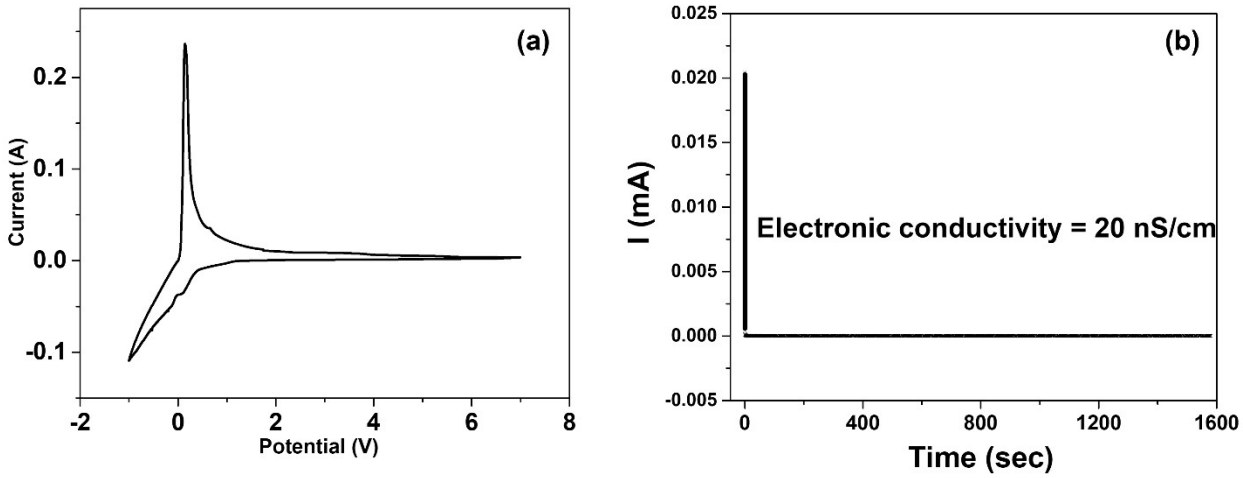

Figure S9 *(a) Cyclic voltammogram of Au/$Na_{3.65}Zr_{1.675}Zn_{0.2}Mg_{0.125}Si_2PO_{12}$/Na asymmetric cell recorded at 0.5 mV/s from –1 to 7 V and (b) DC-polarization test of Au/$Na_{3.65}Zr_{1.675}Zn_{0.2}Mg_{0.125}Si_2PO_{12}$/Au.*

The electrochemical window (shown in Figure S8(a)) of Zn,Mg-codoped NASICON was tested by cyclic voltammetry (CV) of an asymmetric cell (Na/$Na_{3.65}Zr_{1.675}Zn_{0.2}Mg_{0.125}Si_2PO_{12}$/Au) at room temperature in the voltage range from −1 to 7 V. Except the two major peaks near the origin that correspond to the plating and stripping of sodium, no other peaks of any oxidation processes were observed up to 7 V. This validates the sodium ion conduction across the electrolyte and indicates that the electrolyte is stable across a wide electrochemical window. Furthermore, it also enables the integration of the electrolyte with high voltage cathodes for high energy density of solid-state batteries. The electronic conductivity of Zn,Mg-codoped NASICON was determined, by performing DC polarization technique (Figure S8 (b)), to be around 20 nS/cm which was five orders of magnitude less than its ionic conductivity. As the undoped NASICON exhibiting similar electronic conductivities (~ 10^{-8} S/cm),[1] the co-doping seems to not have a significant effect on the electronic structure of the material.

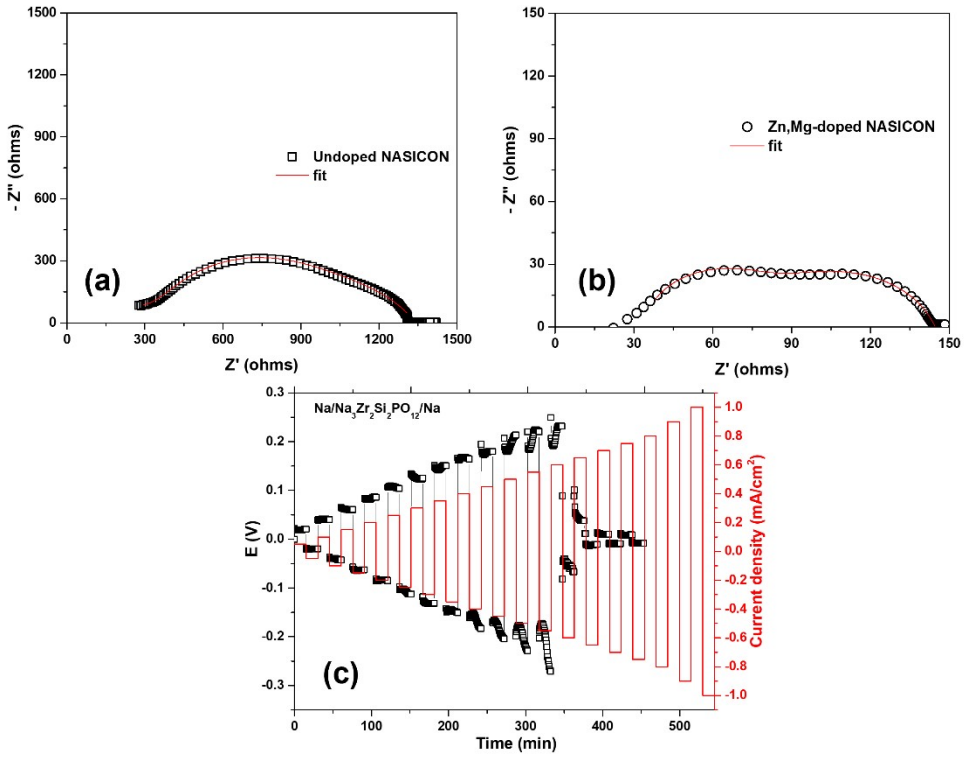

Figure S10 *Nyquist plots of sodium symmetric cells with (a) undoped and (b) Zn,Mg-codoped NASICON dense pellets. (c) Critical current density recorded for the sodium symmetric cell of undoped NASICON.*

Before assembling the cells, the ceramic pellets of undoped and Zn,Mg-codoped NASICON were annealed at 1000 °C for 2 hours to remove any surface functional groups that could affect the interfacial contact with sodium metal.[2] The Nyquist plots of the symmetrical cells with undoped and Zn,Mg-codoped NASICON sandwiched between two sodium metal foils are shown in Figures S9 (a) and (b), respectively. Two coalesced semi-circles were observed from the Nyquist plots, with the high-frequency semi-circle associated with the grain boundary of NASICON and the low-frequency counterpart corresponding to the sodium-NASICON interface. Low interfacial resistances achieved with the symmetric cells indicate that an efficient contact between sodium metal anode and the solid electrolyte in the pellet form was achieved.

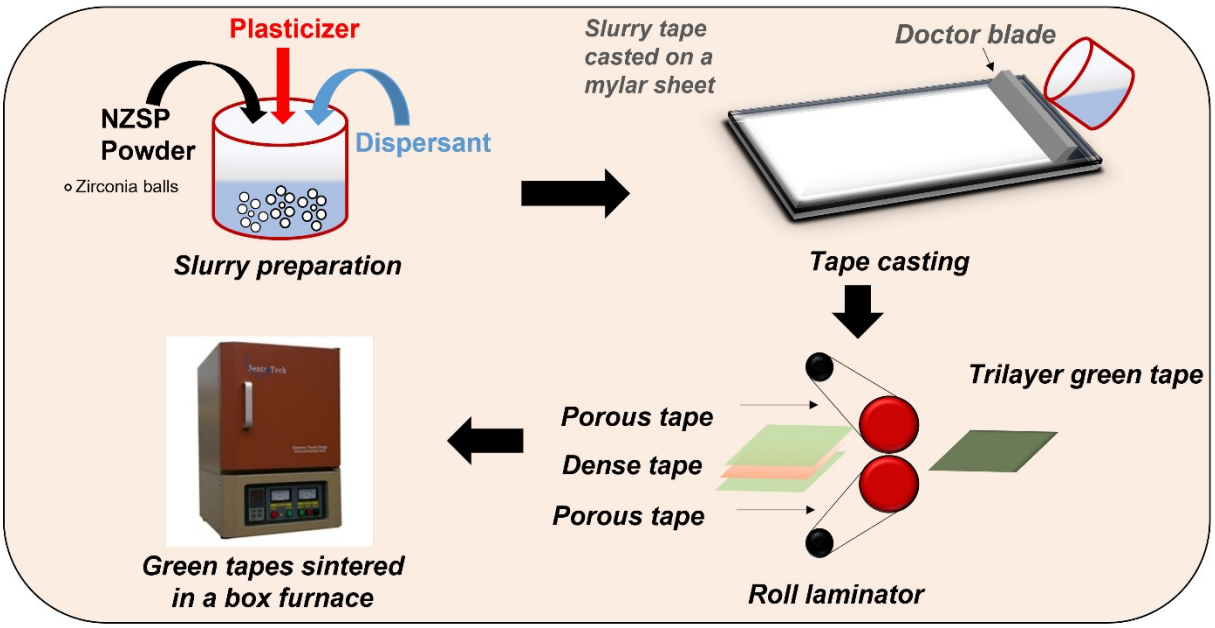

Figure S11 *Schematic of Zn,Mg-codoped NASICON trilayer fabrication*

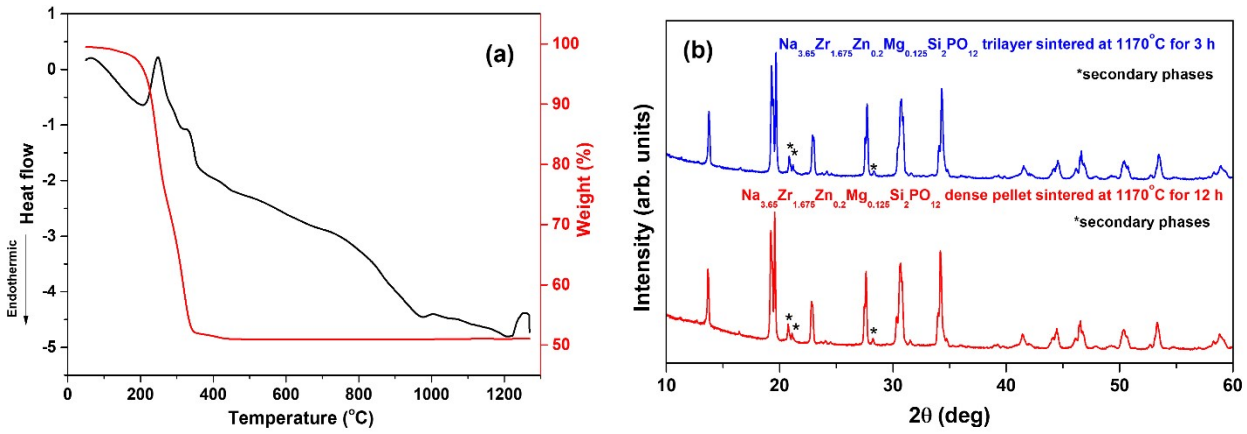

Figure S12 *(a) TGA/DTA curves of trilayer green tape recorded from 50 °C to 1275 °C at a scan rate of 20 °C/min. (b) XRD patterns of sintered trilayer ceramic plates and dense ceramic pellets.*

The thermal properties of the as-laminated trilayer tapes were studied using thermogravimetric/differential thermal analyses (Figure S11 (a)). Below 160 °C, only a minor amount of weight loss was observed which could be associated with release of chemically or physically adsorbed moisture on the green trilayer tape. Between 160 °C and 320 °C, rapid weight loss (around 33 %) due to the decomposition of organic components occurred as corroborated by the exothermic peaks at 250 °C and 290 °C. Beyond 450 °C, no weight loss was observed suggesting a complete burn out of all the filler materials. The endotherms at 950 °C and 1210 °C correspond to melting of secondary phase phophates and Zn,Mg-codoped NASICON, respectively. The optimized sintering temperature was identified as 1170 °C, slightly less than the onset of melting for dual-doped NASICON. XRD pattern of the sintered Zn,Mg-codoped NASICON trilayer suggests that the phase formation is complete without the presence of any tertiary phases (Figure S11 (b)).

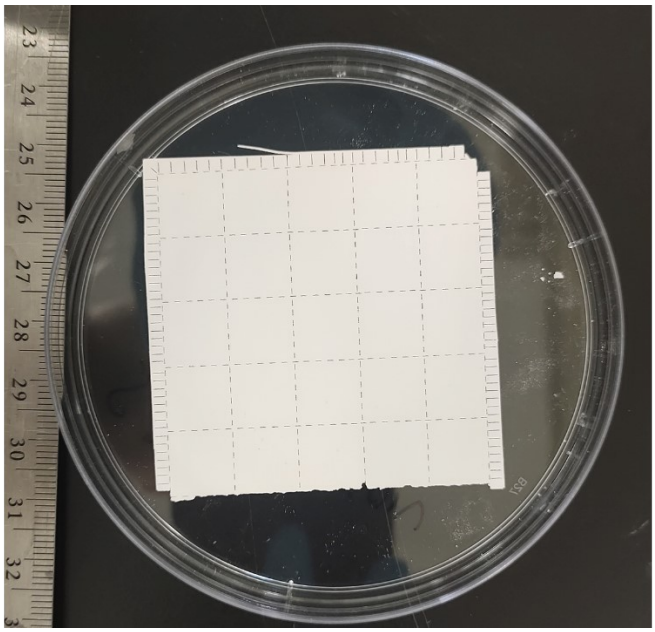

Figure S13 *Photograph of 5x5 set of 1cm² trilayers of Zn,Mg-codoped NASICON composition.*

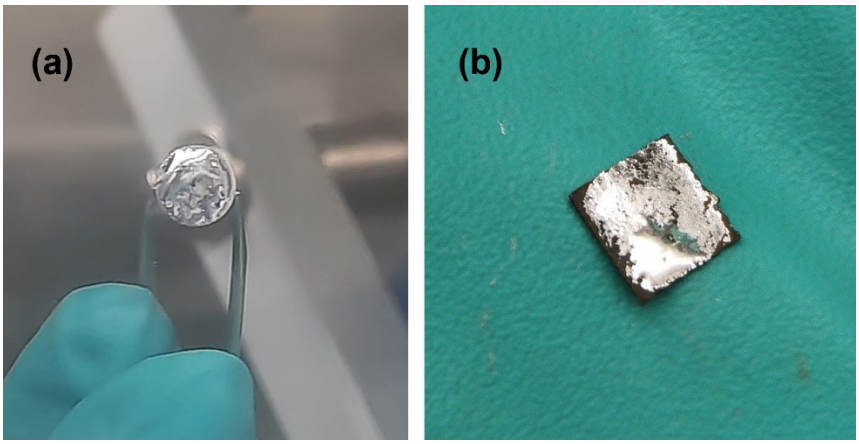

Figure S14 *Optical images of (a) sodium wetted surface of ZnO-coated ceramic pellet and (b) sodium infiltrated trilayer*.

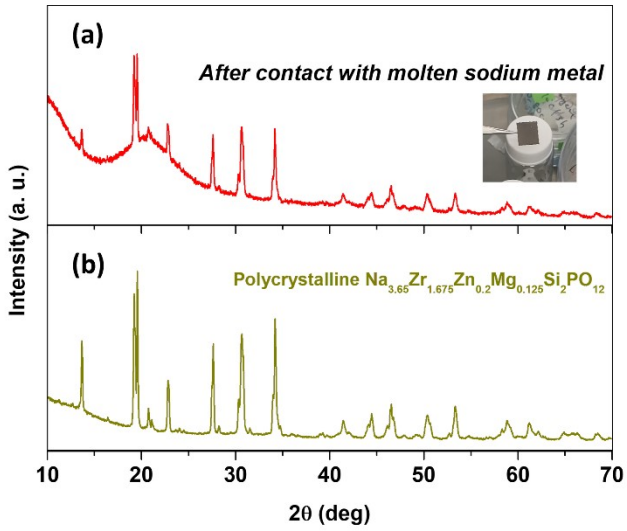

Figure S15 *X-ray diffraction profiles of (a) trilayer after initial contact with molten sodium and (b) polycrystalline Zn,Mg-codoped NASICON composition.*

For this experiment, ZnO-coated porous layer of Zn,Mg-codoped NASICON trilayer was placed over sodium melt and allowed to react over a couple of minutes. The discolored trilayer (as shown in the inset) was taken out of the melt right before the infiltration began. X-ray diffraction of this trilayer was recorded in an argon-filled air-tight dome. This shows that the crystal structure of the Zn,Mg-codoped NASICON trilayer remains intact even after contact with molten sodium. The broad XRD profile observed on the background was due to the dome.

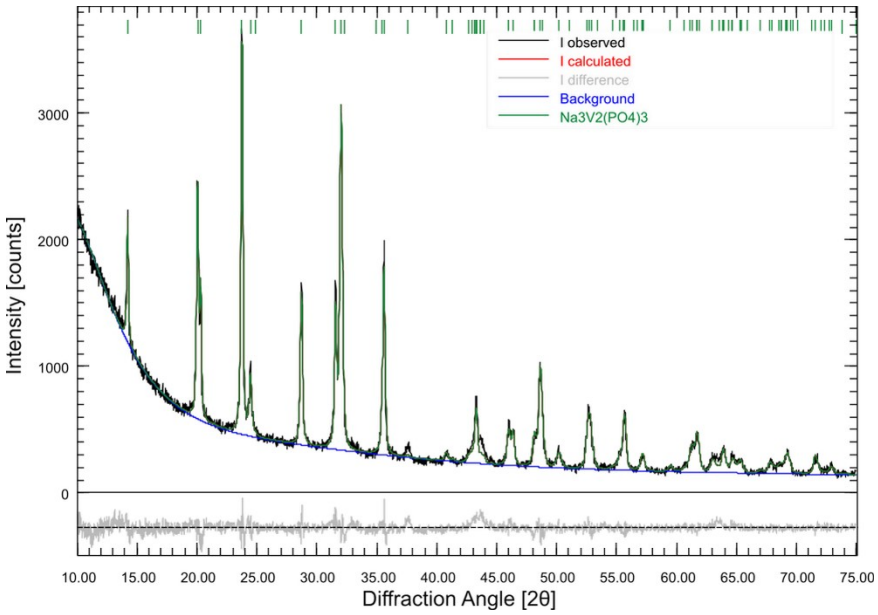

Figure S16 *Rietveld refined X-ray diffraction pattern of sol-gel synthesized* $Na_3V_2(PO_4)_3$.

The XRD pattern (Figure S12) recorded for the as-synthesized powder can be indexed to the pure phase associated with the rhombohedral structure (space group R-3c). The lattice parameters were determined to be a = 0.87 nm and c = 2.18 nm from the Rietveld refinement (R_p = 4.76 %; R_{wp} = 6.46 %) of the XRD profile.

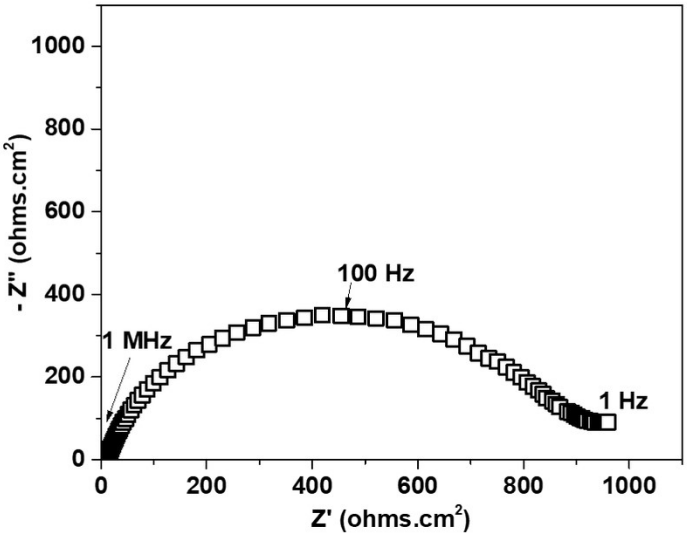

Figure S17 *Impedance plots of Na/Zn,Mg-doped NASICON/NVP at room temperature.*

Table S1. Theoretically achievable energy density using a Zn,Mg-codoped NASICON bilayer and high loading of NVP cathode (5 mAh/cm^2) for a cell of 1 cm^2 area.

Areal weight of the bilayer = 29 mg/cm^2

Area of the bilayer = 1.2 x 1.2 cm^2

Area of the electrodes = 1 cm^2

Thickness of sodium = 80 µm (with respect to the thickness of the porous layer in the solid electrolyte)

Density of sodium = 0.971 g/cm^3

Porosity of the bilayer's porous layer = 65 %

Specific capacity of NVP = 118 mAh/g

Cathode	Electrolyte	Anode	Weight of Cathode (mg)	Loading of NVP (mg)	Weight of Solid Electrolyte (mg)	Weight of Anode (mg)	Capacity (mAh g^{-1})	Average Voltage (V)	Specific Energy (Wh kg^{-1})
NVP	**Zn,Mg-doped NASICON bilayer**	**Na**	**52.5**	**42**	**41**	**5.6**	**118**	**3.4**	**172**

References

1. B. Tang, P. W. Jaschin, X. Li, S-H. Bo, and Z. Zhou, *Mater. Today*, 2020, **41**, 200.
2. J. A. S. Oh, Y. Wang, Q. Zeng, J. Sun, Q. Sun, M. Goh, B. Chua, K. Zeng and L. Lu, *J Colloid Interface Sci.*, 2021, **601**, 418.